Journal of Virology®

VIRUS-CELL INTERACTIONS

Mitochondrial Glycerol-3-Phosphate Dehydrogenase Restricts HBV Replication via the TRIM28-Mediated Degradation of HBx

Canyu Liu,[a,b] Kaitao Zhao,[c] Yingshan Chen,[a,b] Yongxuan Yao,[d] Jielin Tang,[a,e] Jingjing Wang,[c] Chonghui Xu,[a,b] Qi Yang,[a,e] Yi Zheng,[a,b] Yifei Yuan,[a,b] Hao Sun,[a,b] Yongli Zhang,[a] Yuan Zhou,[a] Jizheng Chen,[e] Yun Wang,[a] Chunchen Wu,[g] Rongjuan Pei,[a] Xinwen Chen[a,e,f]

[a]State Key Laboratory of Virology, Wuhan Institute of Virology, Chinese Academy of Sciences, Wuhan, Hubei Province, China
[b]University of Chinese Academy of Sciences, Beijing, China
[c]State Key Laboratory of Virology and Hubei Province Key Laboratory of Allergy and Immunology, Institute of Medical Virology, School of Basic Medical Sciences, Wuhan University, Wuhan, China
[d]Department of Gastroenterology, Guangzhou Women and Children's Medical Center, Guangzhou, China
[e]Guangzhou Laboratory, Guangzhou, China
[f]Guangzhou Medical University, Guangzhou, China
[g]Department of Laboratory Medicine, Maternal and Child Health Hospital of Hubei Province, Tongji Medical College, Huazhong University of Science and Technology, Wuhan, China

ABSTRACT Hepatitis B virus (HBV) infection affects hepatic metabolism. Serum metabolomics studies have suggested that HBV possibly hijacks the glycerol-3-phosphate (G3P) shuttle. In this study, the two glycerol-3-phosphate dehydrogenases (GPD1 and GPD2) in the G3P shuttle were analyzed for determining their role in HBV replication and the findings revealed that GPD2 and not GPD1 inhibited HBV replication. The knockdown of GPD2 expression upregulated HBV replication, while GPD2 overexpression reduced HBV replication. Moreover, the overexpression of GPD2 significantly reduced HBV replication in hydrodynamic injection-based mouse models. Mechanistically, this inhibitory effect is related to the GPD2-mediated degradation of HBx protein by recruiting the E3 ubiquitin ligase TRIM28 and not to the alterations in G3P metabolism. In conclusion, this study revealed GPD2, a key enzyme in the G3P shuttle, as a host restriction factor in HBV replication.

IMPORTANCE The glycerol-3-phosphate (G3P) shuttle is important for the delivery of cytosolic reducing equivalents into mitochondria for oxidative phosphorylation. The study analyzed two key components of the G3P shuttle and identified GPD2 as a restriction factor in HBV replication. The findings revealed a novel mechanism of GPD2-mediated inhibition of HBV replication via the recruitment of TRIM28 for degrading HBx, and the HBx-GPD2 interaction could be another potential therapeutic target for anti-HBV drug development.

KEYWORDS GPD2, HBx, mitochondria, TRIM28, ubiquitin-dependent degradation

Persistent hepatitis B virus (HBV) infections are associated with the development of serious liver diseases, including hepatocellular carcinoma (HCC), fibrosis, cirrhosis, and acute liver failure (1, 2). Despite the availability of safe and effective vaccines for the past 40 years, chronic HBV infection remains a serious threat to global public health, affecting approximately 286 million individuals globally and resulting in 1.5 million new infections annually (3, 4). The current therapeutic strategies using nucleoside/nucleotide analogues and pegylated interferon (IFN)-α have certain limitations, which necessitates the urgent discovery of novel therapeutic strategies for targeting and inhibiting HBV replication to cure chronic hepatitis B (CHB) infections.

The 3.2 kb genome of HBV is one of the smallest and most compact genomes in the *Hepadnaviridae* family (5, 6). The genome comprises a complete minus strand and

Editor J.-H. James Ou, University of Southern California

Address correspondence to Xinwen Chen, chenxw@wh.iov.cn, or Rongjuan Pei, rongjuan_pei@wh.iov.cn.

The authors declare no conflict of interest.

Received 19 April 2023
Accepted 21 April 2023
Published 11 May 2023

an incomplete plus strand (5). After entering the host cell, the relaxed-circular DNA (rcDNA) of HBV translocates to the nucleus, converts into a covalently closed circular DNA (cccDNA), and subsequently assembles into a minichromosome. The minichromosome serves as the template for the synthesis of 3.5-kb, 2.4-kb, 2.1-kb, and 0.7-kb transcripts by the host RNA polymerase II, which is regulated by the HBV promoters, Cp, preS1p, preS2/Sp, and Xp, respectively. The viral genome harbors four overlapping open reading frames (ORFs), namely, C, P, S, and X, which encode the viral core protein (HBcAg), e-antigen (HBeAg), reverse transcriptase/DNA polymerase, surface antigens (L, M, S), and X protein, respectively (6). HBx is a key regulatory protein that regulates both viral replication and host response. Numerous studies have demonstrated that HBx is necessary for initiating and maintaining HBV replication, and that HBx also plays a pivotal role in the pathogenesis of virus-induced HCC (7, 8). HBx is also necessary for the modulation of several host processes, including DNA repair, oxidative stress, metabolism, transcription, signal transduction, protein degradation, cell cycle progression, and apoptosis (9). Targeting the HBx protein can serve as a potential alternative therapeutic strategy for controlling HBV infections and preventing the development of associated diseases.

Owing to the central metabolic role of the liver, the relationship between HBV and metabolic pathways has been investigated in a growing body of research. The findings demonstrated that HBV infections alter the metabolic landscape of hepatocytes. On the other hand, the systematic metabolic alteration of host cells due to viral replication can affect the replication of HBV (10–12). A previous study analyzed the serum metabolomics profile during the clinical phases of CHB, and the findings suggested that HBV might hijack the glycerol-3-phosphate (G3P) shuttle (13), which is mediated by the combined functions of cytosolic glycerol 3-phosphate dehydrogenase (cGPDH, also known as GPD1) and mitochondrial flavin adenine dinucleotide (FAD)-dependent glycerol 3-phosphate dehydrogenase (mGPDH, also known as GPD2). However, it remains to be elucidated whether the G3P shuttle affects the replication of HBV. Additionally, the mechanism by which the G3P shuttle might affect HBV replication remains to be investigated. The mitochondrial GPDH (GPD2) protein, located in the outer leaflet of the mitochondrial inner membrane, is the rate-limiting enzyme in the G3P shuttle. Using FAD as a cofactor, GPD2 catalyzes the conversion of G3P to dihydroxyacetone phosphate (DHAP) and transfers reducing equivalents into mitochondria, which results in the net oxidation of the NADH produced during glycolysis (14). It has been reported that GPD2 is involved in hepatic gluconeogenesis (15) and lipid metabolism (16), but its role in HBV replication remains to be elucidated.

In this study, we investigated the effect of GPD2 on the replication of HBV both *in vivo* and *in vitro*. The results demonstrated that GPD2 inhibits the replication of HBV by promoting the proteasomal degradation of HBx via the TRIM28 E3 ubiquitin ligase.

RESULTS

GPD2 and not GPD1 inhibits HBV replication. Using different HBV replication models and cellular models of HBV infection, we first analyzed whether GPD1 and GPD2, the two components of the G3P shuttle, are involved in the replication of HBV. The levels of HBV replication were first analyzed in the HepG2.2.15 cell line by detecting the levels of HBsAg and HBeAg in the supernatant, and the intracellular levels of HBV RNA, core-associated DNA, and capsid protein were subsequently determined. As depicted in Fig. 1A and B, the knockdown of GPD2 and not GPD1 significantly enhanced the HBV replication levels in HepG2.2.15 cells. The level of HBV replication was subsequently detected in an HBV plasmid transient-transfection system (Fig. 1C and D). The knockdown of GPD2 expression significantly increased the levels of HBsAg, HBeAg, HBV RNA, and core-associated DNA, and the expression of HBV capsid protein in Huh7 cells, while GPD1 knockdown induced a slight relative increase in the HBV replication levels. The precise role of GPD2 in HBV replication was further investigated by overexpressing both GPD1 and GPD2 in Huh7 cells, together with the pSM2 HBV replication plasmid. The overexpression of GPD2 decreased the levels of HBsAg, HBeAg, intracellular HBV RNA, and core-associated HBV DNA, while GPD1

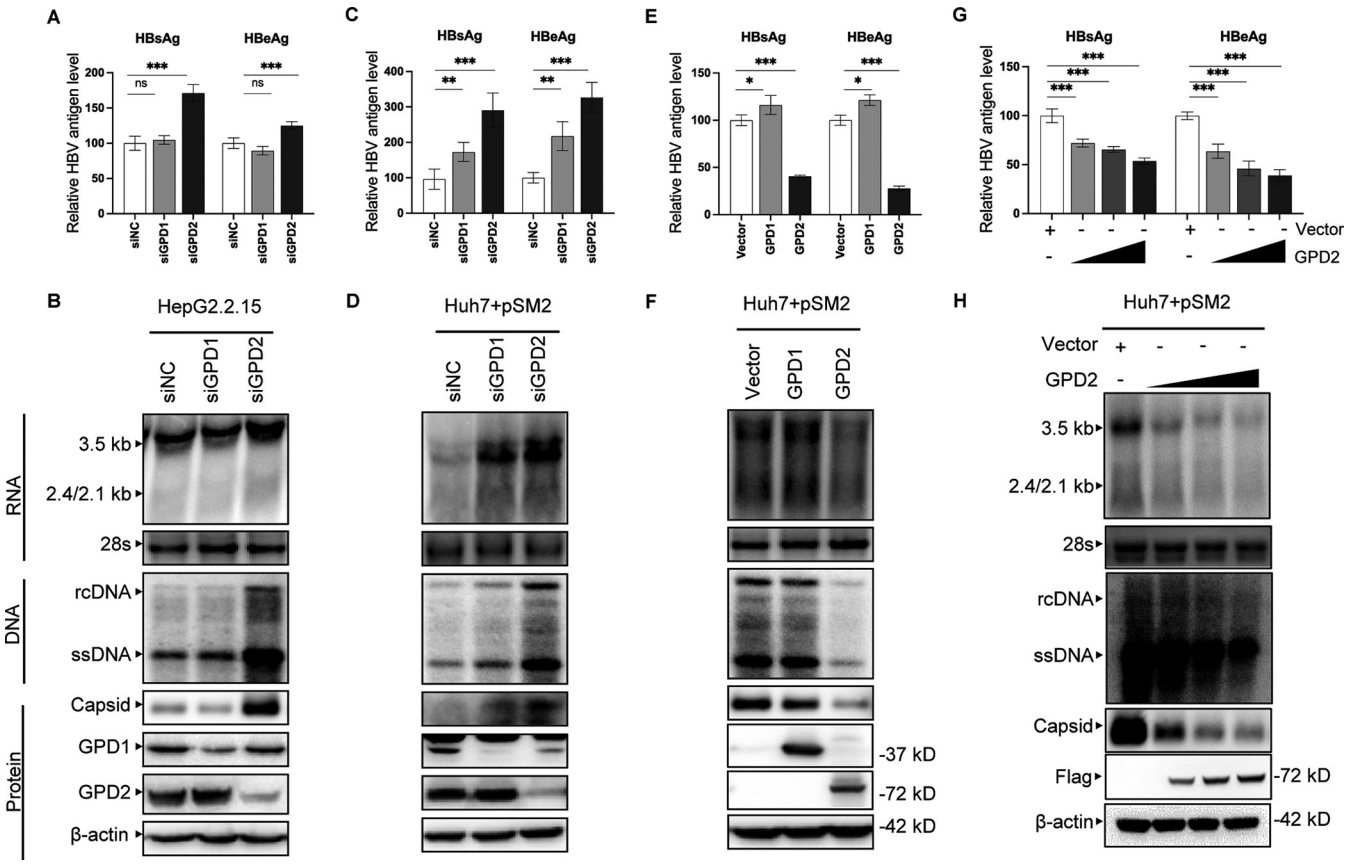

FIG 1 GPD2 and not GPD1 inhibits HBV replication. The cells transfected with siRNAs or plasmids were harvested at 72 hpt. The cell culture supernatants were harvested and analyzed by ELISA ($n \geq 3$). The HBV transcripts were detected by Northern blotting. The 28S rRNA served as the loading control. The positions of the 3.5-kb, 2.4-kb, and 2.1-kb HBV RNA are indicated in the upper panels. The HBV replication intermediates were detected by Southern blotting. The positions of the relaxed circular (RC) and single-stranded (SS) DNA are indicated in the middle panels. The expression of GPD1, GPD2, and Flag and the formation of the viral capsid in the cells was analyzed by Western blotting (lower panels). β-actin served as the loading control. (A and B) HepG2.2.15 cells transfected with siRNAs. (C and D) Huh7 cells were transfected with the indicated siRNAs and subsequently transfected with the HBV replication-competent pSM2 plasmid. (E and F) Huh7 cells were cotransfected with pSM2 and constructs expressing GPD1 or GPD2 proteins, or the empty vector. (G and H) Huh7 cells were transfected with pSM2 and GPD2-Flag or the Flag empty vector, as indicated. The differences between two groups were determined by two-tailed *t* tests or one-way ANOVA followed by Tukey's post hoc test for multiple comparisons (G), and data are represented as mean ± SD (*, $P < 0.05$; **, $P < 0.01$; ***, $P < 0.001$; ns, not significant).

overexpression didn't induce significant alterations in the levels of HBV RNA and DNA but increased the levels of HBeAg and HBsAg by approximately 20% (Fig. 1E and F). The impact of GPD2 on HBV replication was also verified in HepG2 cells, showing that GPD2 silencing increased HBV replication and GPD2 overexpression inhibited HBV replication (see Fig. S1 in the supplemental material). Furthermore, GPD2 overexpression suppressed HBV replication in a dose-dependent manner (Fig. 1G and H). Based on these results, we focused on determining the role and mechanism of action of GPD2 in HBV replication in the subsequent experiments.

An *in vitro* model of HBV infection was generated to understand the role of GPD2 in the natural life cycle of HBV. Huh7D^{hNTCP}-40, a highly permissive cell clone selected from Huh7D^{hNTCP} cells (17), was transfected with pGPD2 and subsequently infected with HBV virions. Consistent with the previous results, the overexpression of GPD2 in Huh7D^{hNTCP}-40 cells decreased the levels of secreted HBV antigens in the supernatant and the levels of intracellular HBV core-associated DNA, HBV RNA, and core protein at 7 days postinfection (dpi) (Fig. 2A and B). In contrast, the silencing of GPD2 expression in Huh7D^{hNTCP}-40 cells elevated the levels of HBeAg and HBsAg in the cell culture supernatant and increased the intracellular levels of core-associated DNA, HBV RNA, and core protein (Fig. 2C and D). Similarly, the overexpression of GPD2 inhibited HBV replication in HepG2-NTCP cells (Fig. S1E and F). The rescue of GPD2 protein expression in siRNA-treated cells by plasmid

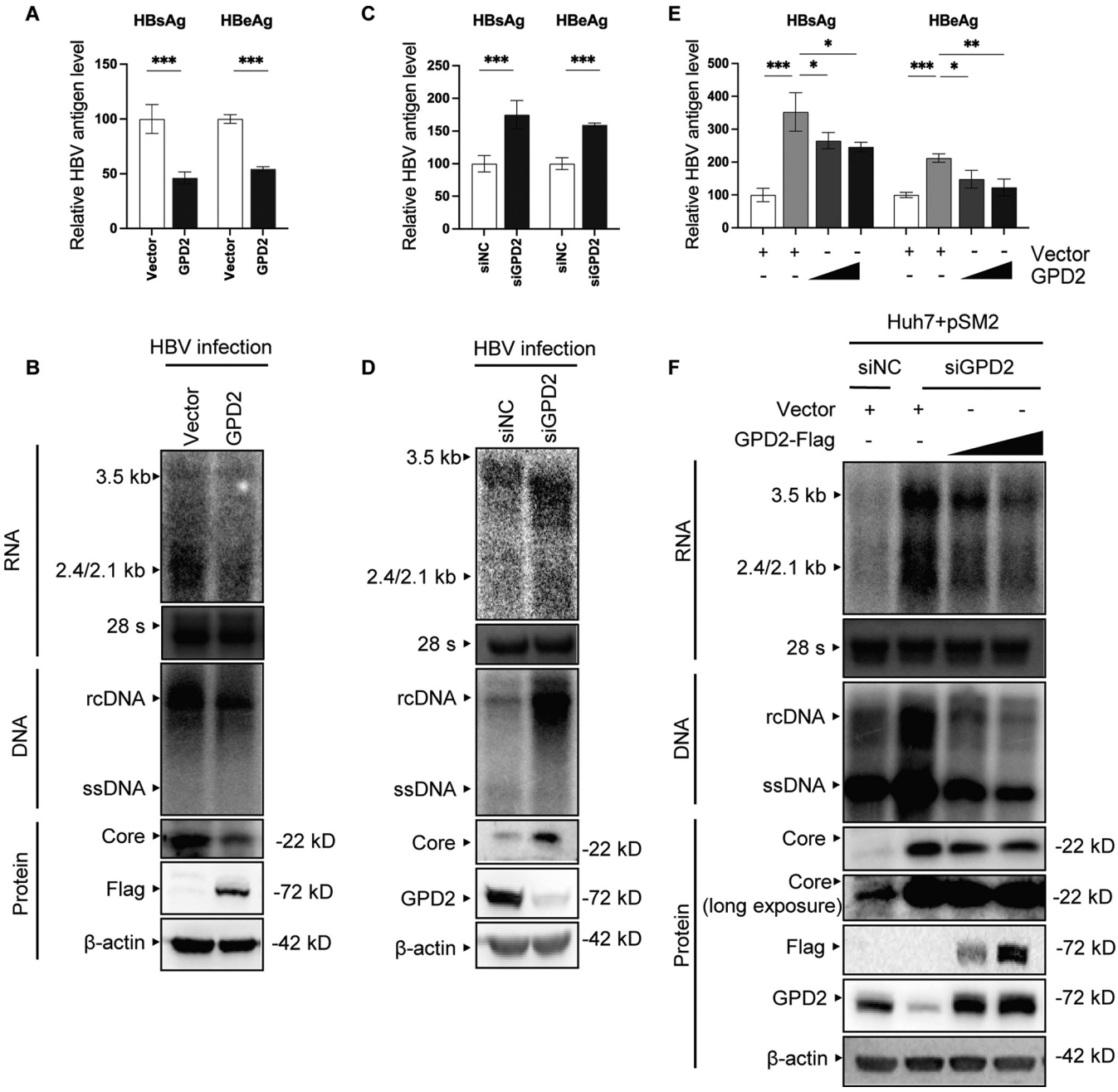

FIG 2 GPD2 inhibits HBV infection and replication. Huh7 and Huh7D^{hNTCP}-40 cells transfected with the indicated plasmids or siRNAs were harvested at 72 hpt or 7 dpi. The supernatants were harvested and analyzed by ELISA ($n \geq 3$). HBV RNAs were detected by Northern blotting (upper panels). The 28S rRNA served as the loading control. The HBV DNA was detected by Southern blotting (middle panels). The expression of GPD2 and core protein in the cells was analyzed by Western blotting (lower panels); β-actin served as the loading control. (A and B) Huh7D^{hNTCP}-40 cells were transfected with the empty vector or GPD2-Flag for 24 h, following which, the cells were inoculated with 500 VGE of HBV and incubated for 16 h. Following infection, the cells were washed thrice with PBS and maintained in the medium for 7 days; the medium was replaced every 2 days. The supernatant and cells were collected for detecting the levels of HBV DNA, RNA, HBsAg, and HBeAg. (C and D) Huh7D^{hNTCP}-40 cells were transfected with siNC or siGPD2, and subsequently infected with HBV. (E and F) Huh7 cells were transfected with siNC or siGPD2 for 24 h, and subsequently cotransfected with pSM2 and the empty vector or GPD2-Flag. The cells and culture supernatants were harvested after 72 h. The differences between two groups were determined by two-tailed *t* tests or one-way ANOVA followed by Tukey's *post hoc* test for multiple comparisons, and the data are represented as mean ± SD (*, $P < 0.05$; **, $P < 0.01$; ***, $P < 0.001$).

overexpression revealed that the upregulation of HBV replication level subsided as the expression of GPD2 was rescued (Fig. 2E and F). Altogether, the findings indicated that GPD2 functions as a restriction factor for HBV replication.

GPD2 inhibits HBV replication in hydrodynamic injection-based mouse models. The inhibitory effect of GPD2 on HBV replication was further evaluated *in vivo* by hydrodynamic injections with the HBV replication-competent pSM2 and pGPD2

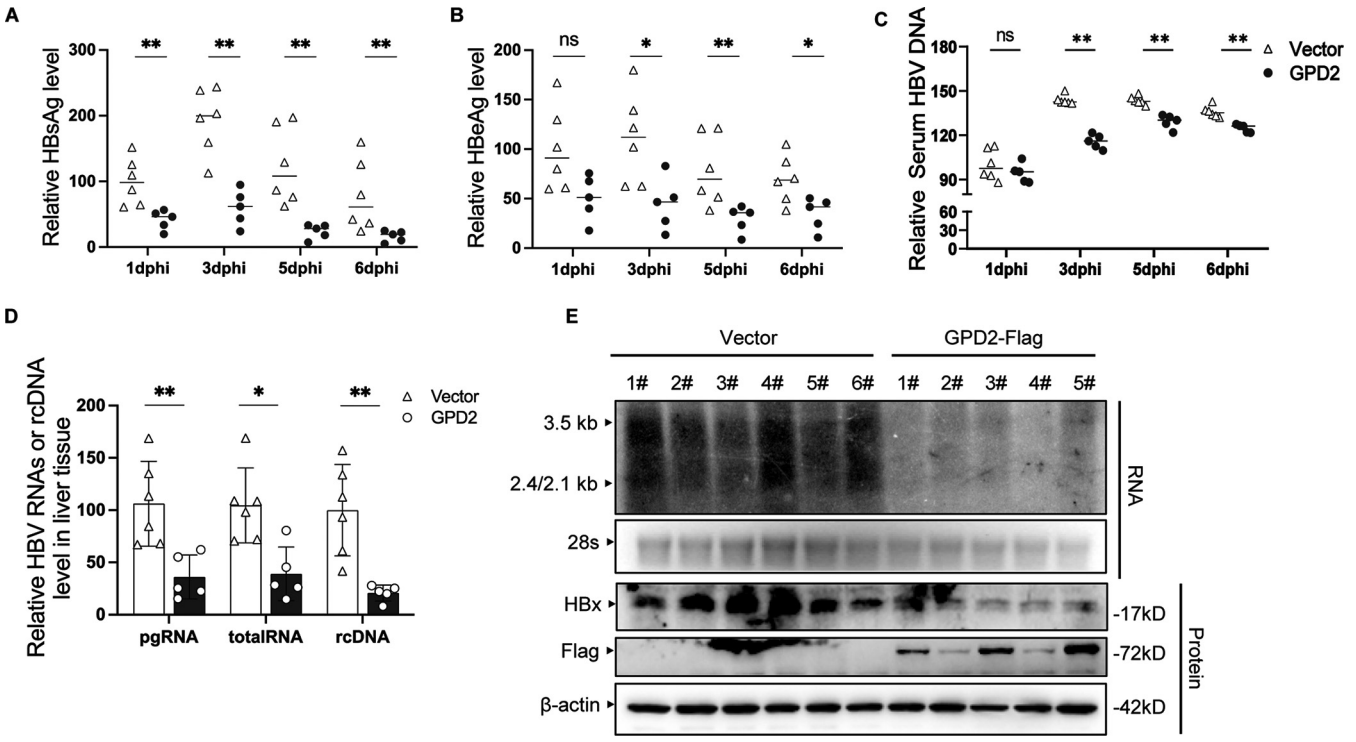

FIG 3 GPD2 inhibits HBV replication in hydrodynamic injection-based mouse models. (A and B) The serum levels of secreted HBsAg and HBeAg were measured with ELISA. (C) The copy numbers of the HBV DNA in the serum were detected by RT-PCR. (D) The levels of HBV RNA and DNA in the liver tissues were analyzed by qRT-PCR after 6 dphi. The RNA levels were normalized to the levels of mouse actin mRNA. (E) The HBV RNA was analyzed by Northern blotting hybridization and the expression levels of HBx and GPD2 in the liver tissues of mice were analyzed by Western blotting. The differences between two groups were determined by Mann-Whitney test (*, $P < 0.05$; **, $P < 0.01$; ***, $P < 0.001$).

plasmids or the empty vector into C57BL/6 mice. Compared to the vector injection group, pGPD2 injection significantly decreased the serum levels of HBsAg, HBeAg, and HBV DNA from 1 day posthydrodynamical-injection (dphi) to 6 dphi (Fig. 3A–C). The serum levels of HBV antigen (HBsAg and HBeAg) and HBV DNA increased and peaked at 3 dphi in the group injected with the empty vector, while the serum levels of HBV antigen remained relatively low from 1 to 6 dphi in the pGPD2 injection group. The level of HBV DNA increased in the group treated with pGPD2 and peaked at 5 dphi. The findings suggested that GPD2 expression reduced and retarded the release of HBV DNA into the serum. The levels of HBV DNA and RNA in the liver tissues were detected by RT-PCR and Northern blotting at 6 dphi. The results demonstrated that the levels of HBV DNA and RNA in the liver tissues were reduced in the pGPD2 injection group (Fig. 3D and E). Interestingly, the overexpression of GPD2 significantly decreased the expression levels of HBx protein in the liver (Fig. 3E). These findings confirmed that GPD2 inhibited the replication of HBV *in vivo*.

The suppression of HBV replication was not related to the catalytic activity of GPD2. We subsequently analyzed whether the catalytic activity of GPD2 is necessary for inhibiting HBV replication. The GPD2-FADmut mutant with reduced enzymatic activity was generated by mutating Gly to Arg at positions 77, 78, and 81 and Thr to Pro at position 90 in the FAD domain, as previously described (18, 19). As GPD2 is a calcium-dependent enzyme (20), calcium-binding domain depletion constructs were also generated in this study (Fig. 4A). Surprisingly, the inhibitory effect of these mutants on HBV replication was similar to that of wild-type (WT) GPD2 in Huh7 cells transfected with pSM2, indicated by the reduction in the levels of HBsAg, HBeAg, and HBV RNA in the cells transfected with these mutants (Fig. 4B and C). Serial truncates of GPD2 were constructed and their effect on HBV replication was subsequently evaluated. The findings revealed that the expression of the N-terminal 1 to 99 residues of GPD2 was sufficient for restricting the replication of HBV, while the other truncates of GPD2 had no

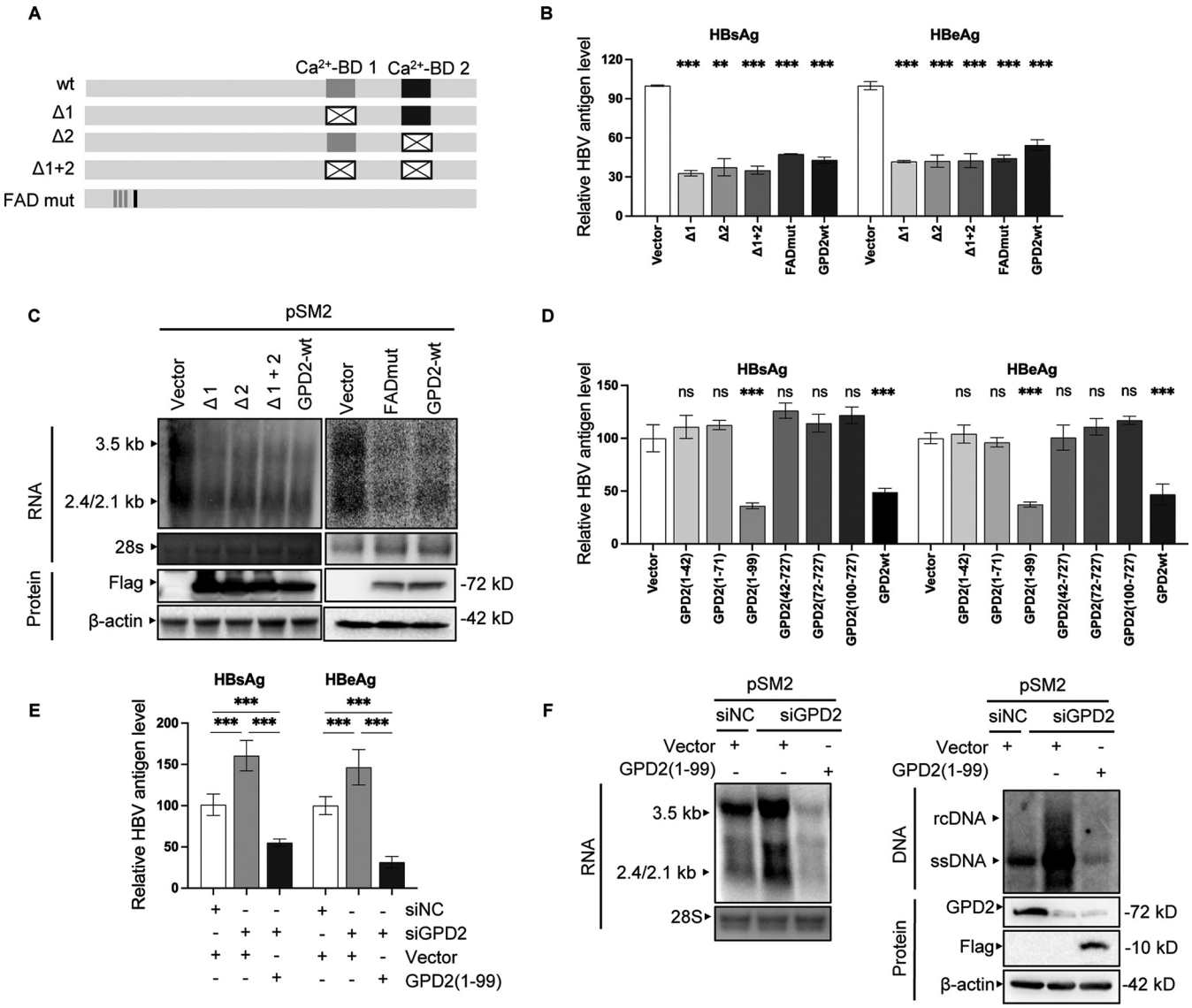

FIG 4 The catalytic activity of GPD2 is not related to the suppression of HBV replication. (A) Schematic diagram depicting the deletion mutants of GPD2: GPD2-Δ1 (Ca^{2+} binding domain 1, Ca^{2+}-BD 1), GPD2-Δ2 (Ca^{2+} binding domain 2, Ca^{2+}-BD 2), GPD2-Δ1+ Δ2, and FAD mutants (Gly to Arg substitution at positions 77, 78, and 81, and Thr to Pro substitution at position 90). (B) Huh7 cells were cotransfected with pSM2 and either the GPD2-derived constructs or the empty vector as indicated and harvested at 72 hpt. The levels of HBsAg and HBeAg were measured using ELISA ($n \geq 3$). (C) The intracellular levels of HBV RNA were quantified by Northern blotting. (D) Huh7 cells were cotransfected with pSM2 and pFlag or the indicated plasmids, and subsequently harvested at 72 hpt. Measurement of the levels of HBsAg and HBeAg by ELISA ($n \geq 3$). (E) The levels of HBeAg and HBsAg in the cell culture supernatants were detected by ELISA ($n \geq 3$). (F) The intracellular expression of HBV DNA, RNA, and HBV proteins was detected. The differences between two groups were determined by two-tailed *t* tests or one-way ANOVA followed by Tukey's *post hoc* test for multiple comparisons, and the data are represented as mean ± SD (*, $P < 0.05$; **, $P < 0.01$; ***, $P < 0.001$).

effect on HBV replication (Fig. 4D). The truncated GPD2 protein (1 to 99) was subsequently overexpressed in siGPD2-treated cells and the findings revealed that the siGPD2-mediated increase in HBV replication was completely reversed by the truncated GPD2 protein (Fig. 4E and F). These findings suggested that the inhibitory effect of GPD2 on HBV replication is independent of its enzymatic activity.

GPD2 inhibits HBV replication by enhancing HBx degradation. To elucidate the mechanism underlying the regulation of HBV replication, we analyzed the interactions of the GPD2 protein with the proteins of HBV. The findings revealed that GPD2 specifically coimmunoprecipitated with HBx but not with other viral proteins. The interaction between GPD2 and HBx was confirmed by coimmunoprecipitation (co-IP) and reverse co-IP assays of Huh7 cells transfected with pSM2, as depicted in Fig. 5A. The immunofluorescence assay additionally revealed that HBx colocalized with the mitochondria proteins in approximately 50% of

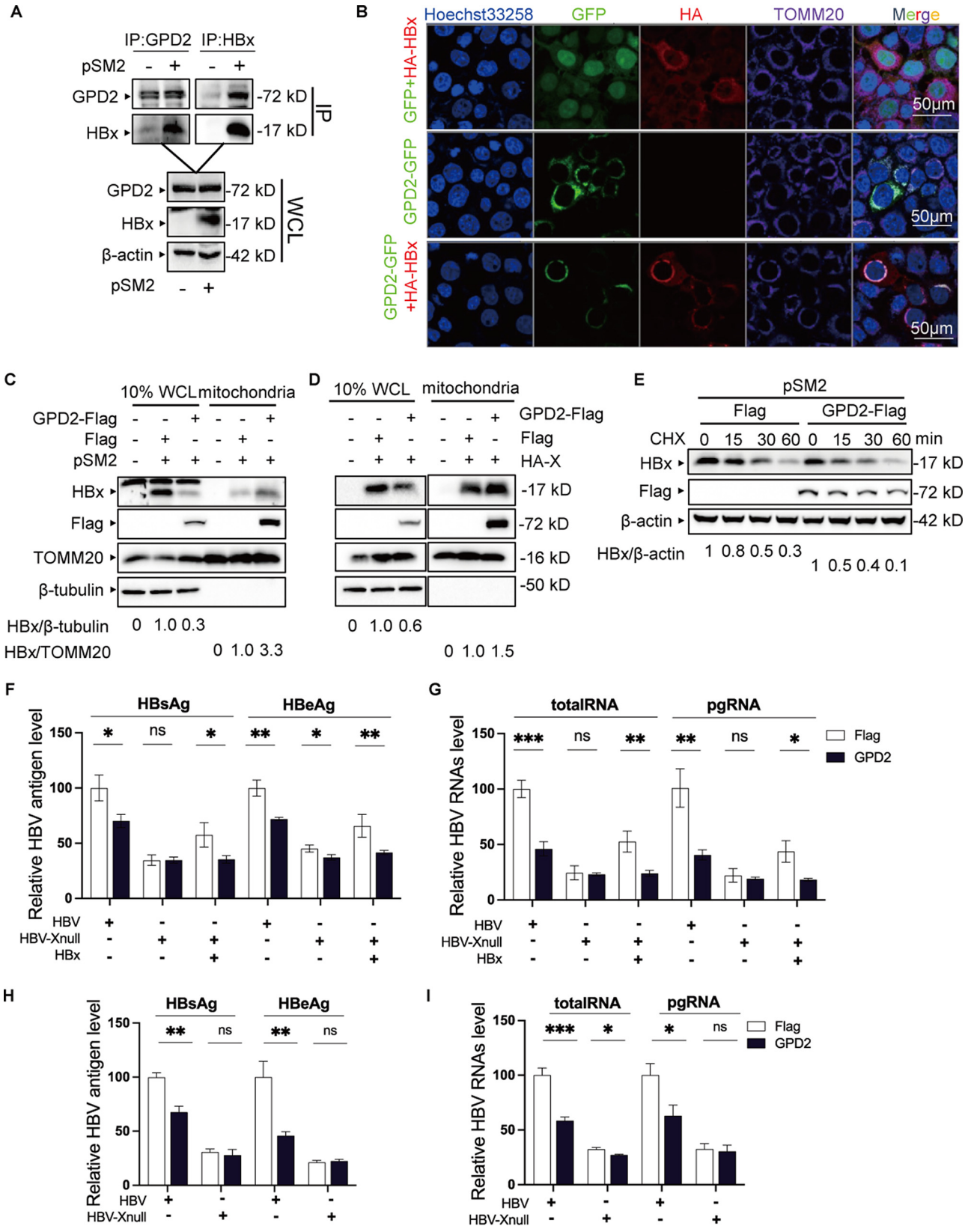

FIG 5 GPD2 inhibits HBV replication by enhancing HBx degradation. (A) Huh7 cells were transfected with pSM2 or the empty vector. The cells were harvested after 24 h and immunoprecipitated with anti-HBx or anti-GPD2 antibodies. Subsequent analysis was performed by immunoblotting (IB) with the corresponding antibodies. (B) Huh7 cells were transfected with HA-X and GPD2-GFP or GFP for 24 h. The interaction between HBx and GPD2 was detected by immunofluorescence staining. Representative composite confocal images depicting GPD2-GFP or GFP (green), HA-HBx (red),

(Continued on next page)

coexpressing GPD2 and HBx cells (Fig. 5B). The average Pearson's correlation coefficient of GPD2 and HBx was 0.7, suggesting that GPD2 colocalizes with HBx. The mitochondrial localization of HBx in Huh7 cells transfected with pSM2 was evaluated by mitochondrial fractionation followed by Western blotting. The overexpression of GPD2 dramatically increased the level of HBx in the mitochondrial fraction; however, the expression level of HBx reduced significantly in the whole-cell lysates (Fig. 5C). As the reduction in HBx levels could be attributed to a reduction in HBV replication, the expression of HBx was subsequently analyzed in Huh7 cells cotransfected with pHBx and pGPD2. Compared to that of the vector control group, the total amount of HBx decreased in the whole-cell lysates but increased in the mitochondrial fraction of cells overexpressing GPD2 (Fig. 5D). As HBx is an unstable protein with a rapid turnover, the stability of the HBx protein was investigated by inhibiting protein synthesis with cycloheximide (CHX). As depicted in Fig. 5E, the overexpression of GPD2 accelerated HBx degradation, which indicated that GPD2 modulates the stability of HBx. The role of HBx in the GPD2-mediated inhibition of HBV replication was subsequently investigated using HBx-null HBV replication plasmids in Huh7 and HepG2 cell line (Fig. 5F–I). As expected, HBV replication markedly decreased in the absence of HBx, which could be partially rescued by the transcomplementation of HBx. Although GPD2 inhibits the replication of WT HBV, this regulatory effect was not observed in HBx-null replicons. The overexpression of GPD2 inhibited HBx-null HBV replication with the transcomplementation of HBx. These findings suggested that HBx is essential for the GPD2-mediated inhibition of HBV replication.

GPD2 promotes HBx degradation via the proteasomal pathway. To characterize the GPD2-mediated pathway of HBx degradation, the cells were treated with the MG132 proteasome inhibitor, CQ lysosome inhibitors, and the autophagy inhibitor, 3-Methyladenine (3-MA) and incubated for 4 h. The results of Western blotting revealed that the GPD2-medicated degradation of HBx was rescued by MG132 but not by CQ or 3-MA (Fig. 6A). Consistently, treatment with MG132 restored the levels of HBx protein in HBV-infected cells and cells transfected with pSM2 (Fig. 6B). The level of HBx ubiquitination was reduced by GPD2 knockdown and enhanced by GPD2 overexpression (Fig. 6C). The findings further revealed that GPD2 modulated the K48-specific ubiquitination and not the K63-specific ubiquitination of HBx (Fig. 6D). These results suggested that the GPD2-induced degradation of HBx was mediated via the ubiquitin-proteasome pathway.

The GPD2 interaction site in HBx was subsequently mapped in this study, and the key lysine ubiquitination site was identified. A total of five HBx deletion mutants were constructed, and results of co-IP experiments indicated that the HBx mutant with a deletion in residues 121 to 154 did not interact with GPD2 (Fig. 6E). Additionally, the deletion of residues 121 to 154 of HBx prevented the GPD2-mediated degradation of HBx (Fig. 6F), which indicated that this region is responsible for the ubiquitination of HBx. There are six conserved lysines at positions 91, 95, 113, 118, 130, and 140 of HBx. We constructed HBx mutants by mutating all but retaining a single lysine residue (K-O). As depicted in Fig. 6G, ubiquitin modification occurred in the K95O, K130O, and K140O mutants, suggesting that K95, K130, and K140 are the possible ubiquitination sites in HBx. Interestingly, GPD2 reduced the expression of HBx K140O but did not reduce the expression of K95O or K130O (Fig. 6H), and GPD2 did not reduce the expression of HBx following the K140R mutation (Fig. 6H). Further, while the overexpression of GPD2 inhibited HBx-null HBV replication with the transcomplementation of HBx, this inhibitory effect was relieved when HBX-null replicon was transcomplemented with HBx

FIG 5 Legend (Continued)
nuclei (blue, Hochest33258), and TOMM20 (purple); magnification ×600. TOMM20 served as the mitochondrial marker. (C and D) Huh7 cells were transiently transfected for 48 h with GPD2-Flag and pSM2 or HA-HBx. The cells were separated into whole-cell lysates and mitochondrial fractions, which were subsequently analyzed by Western blotting. TOMM20 was used as the mitochondrial marker, and β-tubulin was used as the cytoplasmic marker. (E) Huh7 cells were cotransfected with pSM2 and the indicated plasmids. The cells were treated with 100 μg/mL CHX at 24 hpt for inhibiting *de novo* translation. The samples of protein were collected at the indicated time points for evaluating the protein levels, as indicated. (F and G) Huh7 cells were cotransfected with constructs expressing GPD2 protein or HBx protein and either pHBV or pHBV-Xnull, as indicated. (H and I) HepG2 cells were cotransfected with constructs expressing GPD2 protein and pHBV or pHBV-Xnull, as indicated. The levels of HBsAg and HBeAg in the supernatant were measured at 48 hpt ($n \geq 3$) and the levels of pgRNA and total RNA in cells were measured by qRT-PCR ($n \geq 3$). The differences between two groups were determined by two-tailed *t* tests and data are represented as mean ± SD (*, $P < 0.05$; **, $P < 0.01$; ***, $P < 0.001$; ns, not significant).

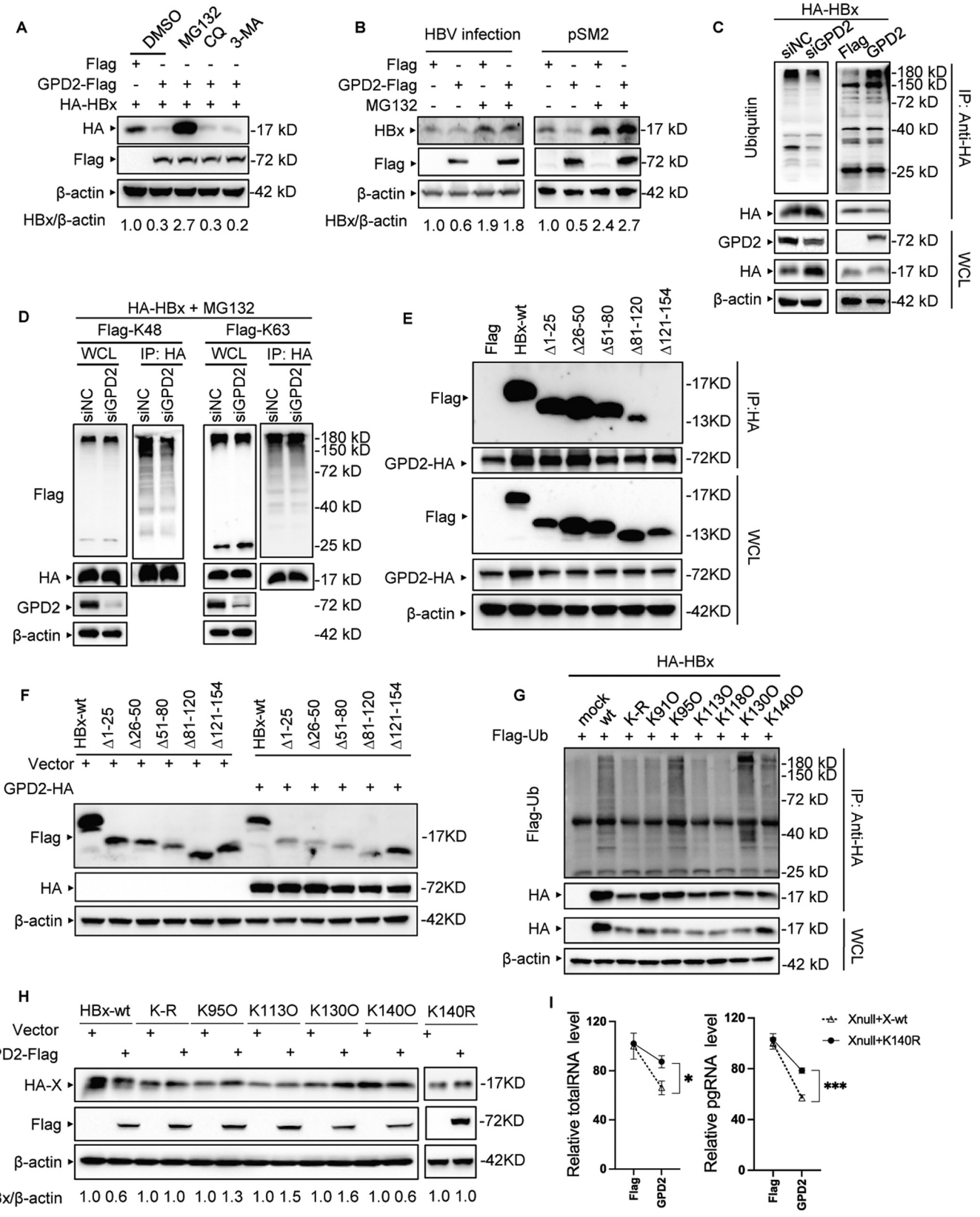

FIG 6 GPD2 promotes HBx degradation via the proteasomal pathway. (A) Huh7 cells were cotransfected with the indicated plasmids and incubated for 24 h. The cells were subsequently treated with MG132 (20 μM), 3-MA (60 μM), or chloroquine (CQ; 50 μM) and incubated for 4 h, and the protein levels were detected by Western blotting. (B) Huh7 and Huh7D^{hNTCP}-40 cells were cotransfected with GPD2-Flag and pSM2 or infected with HBV, as indicated. After 24 hpt or 4 dpi, the cells were treated with MG132 or DMSO for 4 h and the cell lysates were analyzed by Western blotting with the indicated antibodies. (C) The

(Continued on next page)

K140R (Fig. 6I). Altogether, the findings demonstrated that GPD2 triggered the degradation of HBx by promoting ubiquitination at K140.

GPD2 recruits the TRIM28 E3 ubiquitin ligase to degrade HBx. As GPD2 is localized on the mitochondria and increases the amount of HBx on the mitochondria, we assumed that the degradation of HBx could be mediated by the E3 ubiquitin ligases associated with mitochondria. Of the E3 ubiquitin ligase that are reported to mediate the degradation of HBx, the MARCH5, TRIM31, and Siah-1 E3 ubiquitin ligases are either located on the mitochondria or can be recruited to mitochondria (21–23). However, the knockdown of these E3 ubiquitin ligases did not rescue the GPD2-mediated degradation of HBx (Fig. S2A). The mitochondria extracted from Huh7 cells transfected with pSM2 and pGPD2 were coimmunoprecipitated with an HBx antibody and analyzed by mass spectrometry for identifying the proteins that interact with HBx on the mitochondria. Six proteins related to the ubiquitin-proteasome pathway were selected, and their functions in the GPD2-mediated inhibition of HBV were analyzed (Fig. S2B). The E3 ubiquitin ligase TRIM28 was subsequently selected for further studies as the silencing of only TRIM28 partially rescued the levels of HBsAg and HBeAg. The expression levels of HBx were analyzed in cells transfected with pHBx and pSM2. The results demonstrated that the GPD2-induced degradation of HBx was impaired following TRIM28 knockdown (Fig. 7A), and that GPD2 did not reduce the level of K140O HBx in TRIM28 knockdown cells (Fig. 7B). The findings indicated that the TRIM28, a E3 ubiquitin ligase, was responsible for the GPD2-mediated degradation of HBx. We next investigated the interactions among GPD2, TRIM28, and HBx. The results of co-IP experiments indicated that GPD2 interacts with TRIM28 (Fig. 7C) and that GPD2 mediated the interaction between TRIM28 and HBx (Fig. 7D). Additionally, significantly high levels of TRIM28 were detected in the mitochondrial fraction of cells overexpressing GPD2 (Fig. 7E). The replication of HBV was subsequently analyzed in pSM2 transiently transfected Huh7 cells after TRIM28 knockdown, and the findings revealed that the GPD2-mediated inhibition of HBV was suppressed following TRIM28 knockdown (Fig. 7F). Further, after TRIM28 knockdown, the HBV replication in HBV-infected Huh7D$^{hNTCP}-40$ cells was enhanced and the GPD2-mediated inhibition of HBV was relived (Fig. 7G). The findings indicated that GPD2 possibly recruits TRIM28 and forms a complex with HBx in response to HBV infection, which subsequently leads to the proteasomal degradation of HBx (Fig. 8).

DISCUSSION

The relationship between HBV infections and host metabolism involves a wide range of interactions and complex regulatory mechanisms. In this study, we demonstrated that GPD2, an important enzyme of intermediary metabolism, plays a role in the replication of HBV. The knockdown and overexpression of GPD2 *in vitro* and in a hydrodynamic injection-based mouse model demonstrated that GPD2 inhibits HBV replication. The findings also revealed that the enzymatic activity of GPD2 was not essential for its anti-HBV function. Mechanistically, GPD2 inhibited the replication of HBV, possibly by enhancing the interaction of HBx with the E3 ubiquitin ligase TRIM28, which subsequently mediated the K48-linked ubiquitination at K140 and induced the degradation of HBx. The study demonstrated the interactions between HBV infection

FIG 6 Legend (Continued)
ubiquitination of HBx in Huh7 cells transfected with GPD2-Flag and HA-HBx was analyzed by IB assays after 48 h of transfection. (D) Huh7 cells were cotransfected with siRNAs, HA-HBx, and Flag-K48-Ub or Flag-K63-Ub plasmids for 24 h, treated with 20 μM MG132 for 4 h before harvesting. The lysates were immunoprecipitated with anti-HA and subjected to IB assays with anti-Flag and anti-HA. (E) Huh7 cells were cotransfected with the indicated plasmids. After 48 h, the cell lysates were collected and subjected to co-IP assays. (F) The cell lysates were subjected to Western blotting. β-actin was used as the loading control. (G) The expression plasmids encoding HA-HBx or its mutants, in which all lysine residues were mutated to Arg (denoted as K-R). The mutants that retained a single unmutated lysine residue are denoted as K-O. (H) Huh7 cells were cotransfected with GPD2-Flag and HA-HBx or its mutant, harvested at 48 hpt, and analyzed by IB assays. (I) HepG2 cells were transfected with plasmids, as indicated, and harvested at 48 hpt for HBV RNAs quantification by qRT-PCR. The differences between two groups were determined by two-tailed *t* tests or two-way ANOVA followed and Bonferroni's posttest for multiple comparisons, and the data are represented as mean ± SD (*, $P < 0.05$; **, $P < 0.01$; ***, $P < 0.001$).

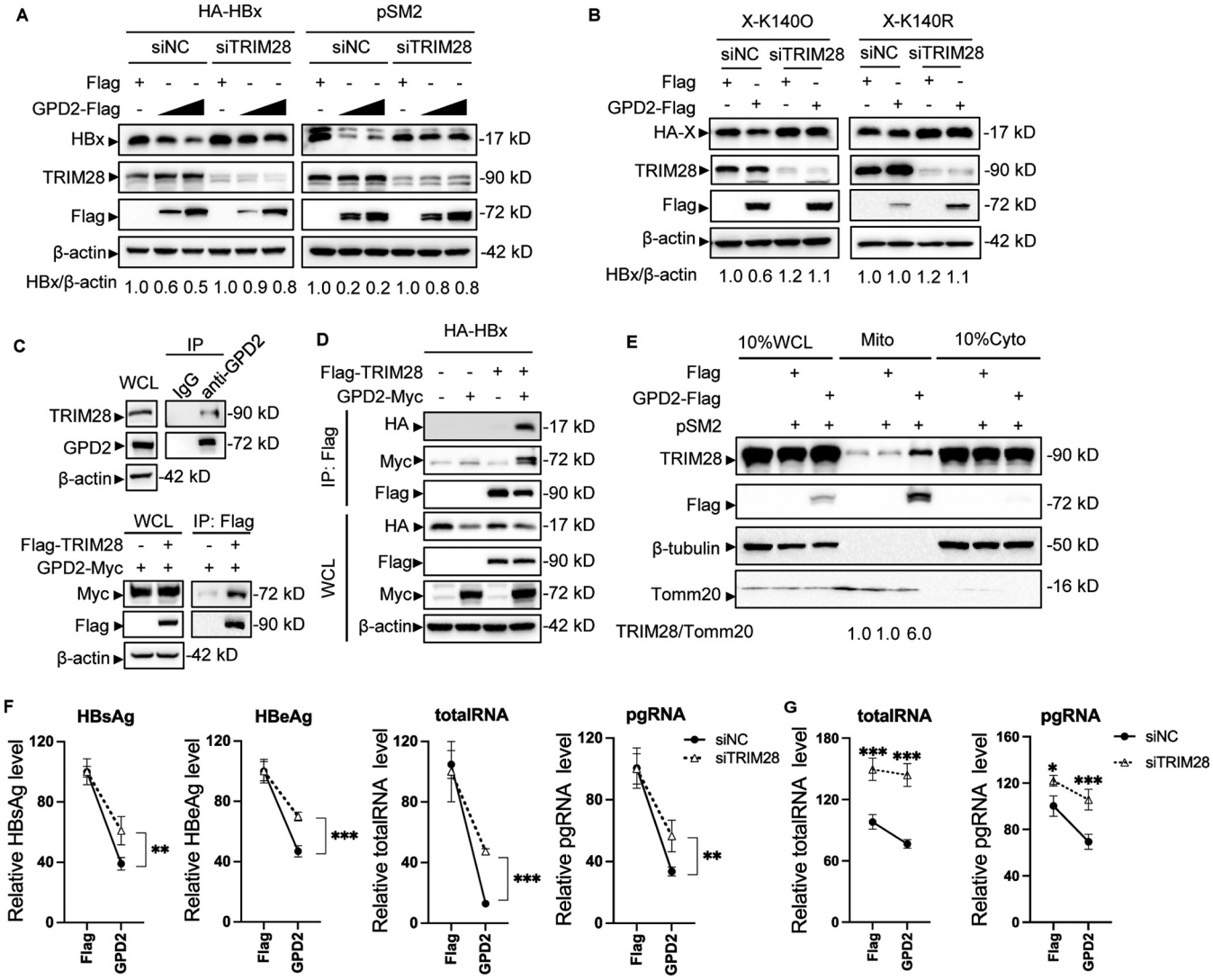

FIG 7 GPD2 recruits TRIM28 to degrade HBx. (A) Cells transfected with siNC or siTRIM28 were cotransfected with GPD2-Myc and HA-HBx or pSM2. The cell lysates were analyzed by Western blotting after 48 h. (B) The cells transfected with siNC or siTRIM28 were cotransfected with the indicated plasmids. The cell lysates were analyzed by Western blotting after 48 h. (C) The cells transfected with the indicated plasmids were subjected to co-IP analysis with anti-GPD2 or anti-Flag. (D) Huh7 cells were transfected with GPD2-Myc, Flag-TRIM28, and HA-HBx for 48 h and subsequently subjected to co-IP assays with anti-Flag. (E) Huh7 cells were transiently transfected with GPD2-Flag and pSM2 for 48 h. The cells were separated into whole-cell lysates, mitochondrial fractions, and cytoplasmic fractions devoid of mitochondria, and subsequently analyzed by Western blotting. TOMM20 was used as the mitochondrial marker and β-tubulin was used as the cytoplasmic marker. (F) Huh7-siNC or siTRIM28 cells were transfected with pSM2 and Flag plasmids or with pSM2 and GPD2 expression plasmids, as indicated. The levels of HBeAg and HBsAg in the supernatants were determined by ELISA at 48 hpt, and the levels of HBV RNA in the cell lysates were determined by qRT-PCR. To show the influence of siTRIM28 on GPD2 function, the HBV RNA and antigen levels in the GPD2-transfected group were normalized to the Flag group. (G) Huh7D^{hNTCP}-40-siNC or siTRIM28 cells were transfected with pGPD2 or Flag plasmids and infected with HBV. Cells were harvested at 7 dpi, and the levels of HBV RNA in the cell lysates were determined by qRT-PCR. The differences between two groups were determined by two-tailed *t* tests or two-way ANOVA followed and Bonferroni's posttest for multiple comparisons, and the data are represented as mean ± SD (*, $P < 0.05$; **, $P < 0.01$; ***, $P < 0.001$).

and the host metabolic pathways and provided novel insights into the mechanisms regulating HBV replication.

HBV infections can induce significant alterations in host metabolism. GPD2 catalyzes the conversion of G3P to DHAP using FAD as a cofactor. The findings demonstrated that GPD2 inhibits HBV replication both *in vitro* and *in vivo*. This might echo the fact that the levels of GPD2 in paracarcinoma liver tissues infected with HBV were lower than those of uninfected tissues (see Fig. S3A in the supplemental material); however, HBV infections did not reduce the expression levels of GPD2 in the hepatoma cell line (Fig. S3B). The findings revealed that the inhibitory effect of GPD2 on HBV replication was independent of its catalytic activity. This was indicated by the fact that the GPD2 mutant with reduced catalytic

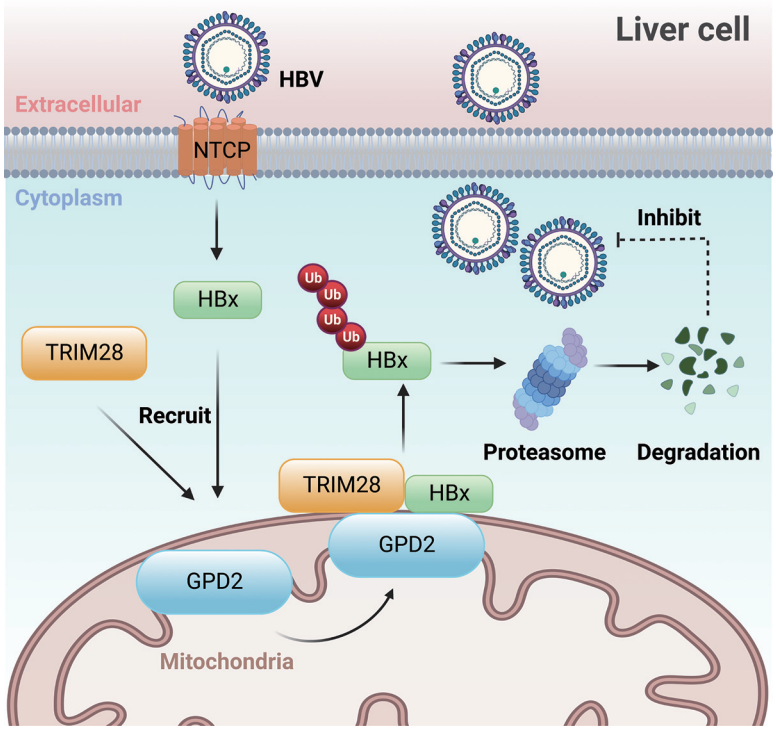

FIG 8 Schematic diagram elucidating the mechanism by which GPD2 inhibits HBV replication. GPD2 recruited HBx and TRIM28 to the mitochondria, forming a complex that then mediated HBx ubiquitination and degraded HBx via the proteasome, allowing GPD2 to inhibit HBV replication.

activity and the truncates that only contained residues 1 to 99 of the N terminus were capable of inhibiting HBV replication. Additionally, though the levels of G3P increased in GPD2 knockdown cells (15), the supplementation of G3P in the cell culture had no influence on HBV replication (Fig. S3C). Furthermore, treatment with 50 μM metformin, which inhibits the activity of GPD2 (15), had no effect on the replication of HBV in this study (Fig. S3D). As metformin has a wide range of regulatory functions (24), the reduction of HBV replication by treatment with a high concentration (5 mM) of metformin (25) could be attributed to the effect of metformin on other pathways and cellular mechanisms. The study further demonstrated that GPD1, the cytosolic component of the G3P shuttle that catalyzes the reversible conversion of DHAP to G3P, is not involved in the replication of HBV. This suggested that alterations in G3P metabolism in hepatoma cell lines does not affect HBV replication. The present study is the first to demonstrate that GPD2, a key factor in G3P metabolism, directly regulates HBV replication.

HBx enhances HBV replication possibly via both direct and indirect mechanisms, and usually functions by cooperating with the cellular signal transduction machinery (26). Previous studies have demonstrated that the deficiency of HBx in the HBV genome, reduction in HBx levels via siRNA treatment, or the promotion of HBx degradation significantly reduce the replication of HBV (7, 27–30). By expressing HBx in cells and cellular models of HBV replication, and using hydrodynamic injection-based mouse models, the present study demonstrated that GPD2 regulates HBV replication by mediating the degradation of HBx. The specific targeting of HBx by GPD2 was further confirmed by an HBx-deficient pHBV plasmid transfection experiment in which the anti-HBV effect of GPD2 was abolished by the deficiency of HBx. Notably, although GPD2 overexpression markedly reduced the total levels and half-life of the HBx protein, the levels of HBx in the mitochondrial fraction increased following GPD2 overexpression. Therefore, the findings indicated that mitochondrial GPD2 may recruit HBx to the mitochondria to mediate its degradation. The results are consistent with several studies which reported that the IFN-induced degradation of HBx suppresses the replication

of HBV (31–34). However, treatment with IFN-α did not upregulate the expression of GPD2 in this study (Fig. S4). As the total level of HBx was reduced following GPD2 overexpression, we assumed that this would suppress the HBx-mediated degradation of SMC5/6 and abolish HBV replication; however, further investigations are necessary in this regard. The balance between the cytosolic and nuclear localization of HBx is influenced by the abundance of HBx, and the HBx-DDB1 interaction contributes to the nuclear retention of HBx (35), which can be enhanced by the NEDDylation of HBx (36). We conjectured that the HBx and GPD2 interaction on the mitochondria could be the cellular mechanism that contribute to the control of HBx subcellular localization.

Several E3 ubiquitin ligases, including TRIM21, TRIM31, MARCH5, NEDD4, and Siah-1, have been reported to mediate the ubiquitination of HBx and target HBx for proteasomal degradation, which further inhibits HBV replication (22, 33, 37–39). Of these, MARCH5, TRIM31, and Siah-1 are either located on the mitochondria or can be recruited to the mitochondria. Although the knockdown of MARCH5, Siah-1, and TRIM31 proteins upregulated the level of HBx protein, the GPD2-mediated degradation of HBx was not rescued following the knockdown of MARCH5, TRIM31, or Siah-1. The present study identified another E3 ubiquitin ligase, TRIM28, which could be recruited to the mitochondria and was responsible for the GPD2-induced degradation of HBx. It has been reported that K90 and K95 are the sites of ubiquitination and degradation in HBx, mediated by TRIM25 (40) and TRIM31 (33), respectively. The findings suggested that GPD2-TRIM28 induced the ubiquitination of HBx at K140. There are several other ubiquitination sites in HBx; however, the mechanism by which ubiquitination is orchestrated at different sites under different physiological conditions remains to be elucidated. The results demonstrated that TRIM28 interacted with GPD2 and was accumulated on the mitochondria during GPD2 overexpression; however, TRIM28 did not interact with HBx in the absence of GPD2. The findings therefore indicated that GPD2 possibly recruits TRIM28 in response to HBV infection and forms a complex with HBx, which leads to the proteasomal degradation of HBx. The GPD2-mediated degradation of HBX observed in this study was consistent with the reports of previous studies which reported that the overexpression of GPD2 increases the ubiquitination and degradation of the Cyp-D protein, which is located in the mitochondrial matrix (16). This also suggests that GPD2, which is a mitochondrial membrane protein, not only regulates cellular metabolism but may also regulate other cellular processes by regulating the stability of target proteins. We also observed that the silencing of TRIM28 was not sufficient for the complete reversal of the inhibitory effect of GPD2 on HBV replication, which indicated that the effect of GPD2 on HBV replication could be mediated via other mechanisms.

Further studies are necessary for determining whether the interaction of HBx with GPD2 affects the enzymatic activity of the latter and further regulates other metabolic pathways. Schoeman et al. (13) proposed that the hijacking of the G3P shuttle by HBV favors the synthesis of plasmalogen lipid species, indicated by an increase in the levels of DHAP-derived plasmalogen phospholipid species, free fatty acids, and acyl carnitines, and a significant reduction in the levels of glycerophospholipids, triglycerides, and sphingomyelins in patients during the immune tolerant phase. GPD2 couples G3P oxidation with ubiquinone reduction to produce ubiquinol, which acts as a radical-trapping antioxidant in mitochondria. The knockdown of GPD2 in hepatocytes decreases the NAD^+/NADH ratio and inhibits the production of mitochondrial reactive oxygen species (ROS), but increases the content of G3P and triglycerides, which induces the accumulation of lipid droplets (15, 16, 41). The HBx-induced production of ROS induces and promotes chronic liver disease and HCC (42), and the interaction of HBx with GPD2 could play a crucial role in the progression of liver disease.

The HBx protein is a potential therapeutic target for drug development against HBV. Several studies have attempted to screen anti-HBV compounds that target HBx. For instance, it has been reported that rapamycin and dicoumarol significantly reduce the expression of HBx and show potent antiviral activity against HBV (30, 43). Another study reported that nitazoxanide functions as an anti-HBV compound by interfering with the interaction of HBx with DDB1 (44). The findings of the present study

suggested that the HBx-GPD2 interaction could be another potential therapeutic target for anti-HBV drug development.

MATERIALS AND METHODS

Cell culture and transfection. The human hepatoma cell lines Huh7, HepG2, HepG2-NTCP, HepG2.2.15, and Huh7D^{hNTCP}-40 were cultured in Dulbecco's modified Eagle's medium (DMEM; Life Technologies) supplemented with 10% (vol/vol) fetal bovine serum (FBS, Gibco, Thermo Fisher Scientific) and penicillin/streptomycin (Life Technologies, 100 units/mL). HepAD38 cells were cultured in a DMEM/F12 (1:1) medium (Gibco) and under the strict control of a tetracycline-responsive promoter. The cells were cultured at 37°C in a humidified incubator with 5% CO_2 and regularly passaged every 2 to 3 days. The Huh7D^{hNTCP}-40 cell clone was selected from Huh7D^{hNTCP} cells which express hNTCP stably (17), and was highly permissive for HBV infection (45, 46).

For cellular transfection, the Huh7, HepG2, HepG2-NTCP, HepG2.2.15, and Huh7D^{hNTCP}-40 cells were seeded in plates and grown to a confluence of 70% the following day. The plasmids were transfected into cells using the Lipofectamine 2000 reagent (Invitrogen) or the Lipofectamine 3000 reagent (Invitrogen), according to the manufacturer's instructions. For most of the experiments, transfection was performed in 6-well plates, and 1-μg aliquots of each of the plasmids were added to each well. To analyze the effect of the dose-dependent expression of GPD2, the cells were separately treated with four doses (0, 0.5, 1.0, and 1.5 μg/well) of GPD2, and the control plasmid was added at a concentration of 1.5 μg/well. The small interfering RNAs (siRNAs) were transfected with Lipofectamine RNAiMAX reagent (Invitrogen), according to the manufacturer's instructions.

Plasmids and siRNAs. The coding sequence of human GPD2 (GenBank accession number: NM_001083112.3) was amplified by PCR. The amplified gene was inserted into the pXJ40 plasmid (Invitrogen, Carlsbad, CA, USA) to generate pXJ40-GPD2-Flag, pXJ40-GPD2-HA, or pXJ40-GPD2-Myc. The HBV replication-competent pHBV1.2 plasmid containing 1.2 copies of the HBV genome and the HBx-depleted pHBV-HBx-null plasmid were kindly provided by Qiang Deng of the School of Basic Medical Sciences, Fudan University. The HBV replication-competent pSM2 plasmid contains a head-to-tail tandem dimer of the HBV genome (genotype D, subtype ayw) and had been described previously (47). HBx truncates were kindly provided by Xu Lin of the Key Laboratory of Gastrointestinal Cancer, Fujian Medical University. TRIM28, HBx were generated by cloning the respective genes into the pXJ40 vector with Flag or HA tag. The siRNAs targeting GPD2 (siGPD2) and TRIM28 (siTRIM28), and the control siRNA (siNC) were purchased from GenePharma (Suzhou, China). The sequences of the siRNAs are as follows: siGPD2: GUAGGAAUCAAGCUGUAUGTT; siTRIM28: ACAGGACAGAGAACAGAGCTT.

HBV virion production and infection. HBV virions (genotype D) were extracted and concentrated with 8% polyethylene glycol (PEG) 8000 (PEG8000) from the culture medium of HepAD38 cells, and subsequently quantified by HBV-DNA real-time PCR (RT-PCR). The HBV infections were conducted as previously reported (48). Briefly, Huh7D^{hNTCP}-40 cells were infected with 500 virus genome equivalent (VGE)/cell of HBV in the presence of 4% PEG8000. After 16 h, the infection inoculum was removed, and the cells were washed thrice with phosphate-buffered saline (PBS). The cells were subsequently maintained in the culture medium with 2% dimethyl sulfoxide (DMSO, Sigma-Aldrich).

Hydrodynamic injections in mice. Male C57BL/6 (H-2b) mice, aged 5 to 6 weeks, were purchased from Beijing HFK Bioscience (China) and maintained under specific-pathogen-free (SPF) conditions at the Central Animal Laboratory of Wuhan Institute of Virology, Chinese Academy of Sciences. All the animal experiments were approved by the Institutional Animal Ethical Committee of WIV, CAS (approval number: WIVA02202103). This study was performed in strict accordance with the recommendations of the Guide for the Care and Use of Laboratory Animals and the regulations in the People's Republic of China.

The hydrodynamic injection-based mouse model of HBV infection was established as previously described (48). Male mice were randomly divided into the control (n = 6) and treatment groups (n = 5) and were hydrodynamically injected with 14 μg pSM2 and 6 μg pGPD2 or the vector diluted in 1.6 mL PBS within 5 to 7 s via the tail vein. The mice were euthanized by cervical dislocation at 6 days posthydrodynamical-injection (dphi). The serum and liver samples of the mice were collected at the indicated time points.

Analysis of HBV replication and transcription. HBV replication intermediates of intracellular core particles were isolated from hepatoma cells and mice liver tissues for analyzing the HBV DNA and detected by Southern blotting or RT-PCR according to published protocols (49). The transfected cells were washed with PBS and lysed in lysis buffer (50 mM Tris-HCl [pH 7.4], 1 mM EDTA, and 1% NP-40) for 10 min on ice. The cellular debris and nuclei were removed by centrifugation for 1 min at 10,000 $\times$ g and the supernatants were digested with 10 mM $MgCl_2$ and 10 mg/mL DNase I (Sigma-Aldrich) for 30 min at 37°C for eliminating the contaminated transfected plasmid DNA. The reaction was ceased by the addition of 25 mM EDTA, following which 0.5 mg/mL proteinase K (Qiagen) and 1% sodium dodecyl sulfate (SDS) were added, and the mixture was incubated at 55°C for 2 h. The HBV-DNA from the intracellular core particles was purified by phenol-chloroform (1:1) extraction and ethanol precipitation. The DNA was washed with 75% ethanol and dissolved in Tris-EDTA (TE) buffer (10 mM Tris-HCl [pH 8.0] and 1 mM EDTA). The DNA samples were resolved in 1% agarose gels and transferred to positively charged nylon membranes (GE Healthcare). The membranes were hybridized with a ^{32}P-labeled full-length HBV probe prepared using a random priming labeling kit (Roche) in hybridization buffer (Invitrogen). The hybridization signals were visualized and analyzed using a Phosphor-Imager system (Cyclon, Perkin Elmer). The rcDNA was detected by RT-PCR using the forward (5′-ACCAATCGCCAGTCAGGAAG-3′) and reverse (5′-ACCAGCAGGGAAATACAGGC-3′′) primers. HBV DNA was extracted from the serum samples

of mice using a DNA blood minikit (Qiagen, 51,106) and quantified by RT-PCR using FastStart universal SYBR green master mix (Roche, 4913914001).

For HBV transcription analysis, HBV RNA was extracted and detected by Northern blotting or one-step quantitative reverse transcription-PCR (qRT-PCR), as previously described (48). Briefly, the total cellular RNA was extracted with TRIzol reagent (Invitrogen) according to the manufacturer's protocol. A 30-μg aliquot of the total RNA was separated by electrophoresis in 1% denaturing agarose gel and subsequently transferred onto a positively charged nylon membrane. Subsequent qRT-PCR analyses were performed using a Quant Studio 6 Flex system (Applied Biosystems) with a QuantiTect SYBR green RT-PCR kit (Qiangen), according to the manufacturer's instructions. The β-actin gene was used as the reference, and the relative mRNA levels were calculated using the $2^{-\Delta\Delta Ct}$ method. The forward (5′-GCCTTAGAGTCTCCTGAGCA-3′) and reverse (5′-GAGGGAGTTCTTCTTCTAGG-3′) pgRNA primer pair and the forward (5′-CCGTCTGTGCCTTCTCATCTGC-3′) and reverse (5′-ACCGACCTTGAGGCATACTT-3′) total RNA primer pair was used in this study.

Western blotting. Western blotting was performed as previously described (38). The following antibodies were used for Western blotting: rabbit anti-HBcAg (Gene Technology, GB058629), rabbit anti-HBx (Biovendor, RD981038100), rabbit anti-GPD2 (Proteintech, 17219-1-AP), rabbit anti-TRIM28 (ABclonal, A2245), mouse anti-β-actin (Proteintech, 66009-1-Ig), rabbit anti-TOMM20 (Proteintech, 11802-1-AP), rabbit anti-ubiquitin (ABclonal, A0162), rabbit anti-Flag (CST, 2368S), rabbit anti-HA (CST, 3724S), and rabbit anti-Myc (Proteintech, 16286-1-AP). The membranes were washed with Tris-buffered saline with Tween 20 (TBST) and incubated with Peroxidase-AffiniPure rabbit anti-mouse IgG antibody (Jackson ImmunoResearch, 315-035-048) or Peroxidase-AffiniPure goat anti-rabbit IgG antibody (Jackson ImmunoResearch, 111-035-045). The antibody-bound protein was detected using a WesternBright ECL HRP kit (Advansta, K-12043-D20).

Immunofluorescence assays. For the confocal laser scanning microscopy experiments, Huh7 cells grown on coverslips were transfected with the indicated plasmids followed by immunofluorescence assays, as previously described (50). The anti-HA (Sigma, H9658) and anti-TOMM20 (Proteintech, 11802-1-AP) antibodies were used as the primary antibodies, and the Alexa Fluor 568-conjugated (Life Technologies, A10037) and Alexa Fluor 633-conjugated (Life Technologies, A21070) antibodies were used as the secondary antibodies. The images were quantified (at least 10 cells per each sample) with Volocity software, version 5.2.

Coimmunoprecipitation assays. The transfected Huh7 cells were lysed with IP buffer at 48 h post-transfection (hpt), and subjected to the coimmunoprecipitation (co-IP) assay, as previously described (51). The anti-Flag (Sigma, F1804) and anti-HA (Sigma, H9658) antibodies were used in the co-IP assays, and mouse IgG (Sigma; I5381) served as the control.

Measurement of HBsAg and HBeAg levels by enzyme-linked immunosorbent assay. The levels of HBsAg and HBeAg in the cell supernatants and sera were assessed by ELISA using Antibody to Hepatitis B Surface Antigen and Antibody to Hepatitis B Virus E Antigen ELISA kits, according to the manufacturer's instructions (Kehua Biotech Co., Ltd., Shanghai, China).

Mitochondrial fractionation. Huh7 cells were transfected with GPD2-Flag or Flag and the pSM2 plasmid for 48 h. The cells were harvested and isolated using a cell mitochondria isolation kit (Beyotime, C3601), according to the manufacturer's instructions. Briefly, the cells were harvested and washed twice with ice-cold PBS. The cells were subsequently incubated in cell lysis buffer for 15 min at 4°C and homogenized with a glass homogenizer. The cell lysate was centrifuged at 800 $\times$ *g* for 10 min to remove any unbroken cells, and the supernatant was further centrifuged at 15,000 $\times$ *g* for 10 min at 4°C. The resulting supernatant contained the cytoplasmic fraction, and the pellet contained the mitochondrial fraction. The mitochondrial pellet was further resuspended in a mitochondrial lysis buffer at 4°C. The concentration of protein in the mitochondrial fraction was measured by the Bicinchoninic acid (BCA) assay (52).

Statistical analyses. Statistical analysis was performed using GraphPad Prism 8.0 software (GraphPad Software Inc., La Jolla, CA, USA). The results are presented as the mean $\pm$ standard deviation ($n \geq 3$). Cell experiments were performed in triplicate, and a minimum of 3 independent experiments were evaluated. The differences between the experimental and control groups were determined by Student's *t* test for comparing two groups of data, one-way ANOVA followed by Tukey's *post hoc* test for multiple comparisons, or two-way ANOVA followed and Bonferroni's posttest for multiple comparisons. The differences were considered statistically significant at $P < 0.05$.

SUPPLEMENTAL MATERIAL

Supplemental material is available online only.

SUPPLEMENTAL FILE 1, PDF file, 0.5 MB.

ACKNOWLEDGMENTS

The authors express their gratitude to Qiang Deng for providing the pHBV1.2 WT and pHBV1.2 HBx-null plasmids, and to Xu Lin for providing the HBx truncation plasmids. We acknowledge He Zhao, Fan Zhang, Li Li, and Xuefang An from the animal experiment center of Wuhan Institute of Virology for their help during the animal experiments. The authors also acknowledge Ding Gao, Anna Du, and Juan Min of the Core Facility and Technical Support, Wuhan Institute of Virology, for their excellent technical support.

X.C., R.P., and C.L. conceived and designed the experiments; X.C., C.W., and R.P. supervised the project; C.L., K.Z., Y.C., Y.X. Yao, J.T., C.X., J.W., Q.Y., Y. Zheng, Y.F. Yuan, H.S., Y.L. Zhang, Y. Zhou, and C.W. performed the experiments and analyzed the data; J.C., Y.W., and R.P. contributed to the interpretation of the results; C.L., R.P., and X.C. prepared the manuscript.

This work was supported by a grant from the National Key Research and Development Program of China (grant number: 2018YFA0507201) and The Pearl River Talent Recruitment Program (grant number: 2019CX01Y422).

The authors have no potential conflicts of interest to declare.

REFERENCES

1. Lavanchy D. 2004. Hepatitis B virus epidemiology, disease burden, treatment, and current and emerging prevention and control measures. J Viral Hepat 11:97–107. https://doi.org/10.1046/j.1365-2893.2003.00487.x.
2. Torres HA, Davila M. 2012. Reactivation of hepatitis B virus and hepatitis C virus in patients with cancer. Nat Rev Clin Oncol 9:156–166. https://doi.org/10.1038/nrclinonc.2012.1.
3. https://www.who.int/news-room/fact-sheets/detail/hepatitis-b.
4. Wong GLH, Gane E, Lok ASF. 2022. How to achieve functional cure of HBV: stopping NUCs, adding interferon or new drug development? J Hepatol 76:1249–1262. https://doi.org/10.1016/j.jhep.2021.11.024.
5. Tsukuda S, Watashi K. 2020. Hepatitis B virus biology and life cycle. Antiviral Res 182:104925. https://doi.org/10.1016/j.antiviral.2020.104925.
6. Tong S, Revill P. 2016. Overview of hepatitis B viral replication and genetic variability. J Hepatol 64:S4–S16. https://doi.org/10.1016/j.jhep.2016.01.027.
7. Lucifora J, Arzberger S, Durantel D, Belloni L, Strubin M, Levrero M, Zoulim F, Hantz O, Protzer U. 2011. Hepatitis B virus X protein is essential to initiate and maintain virus replication after infection. J Hepatol 55:996–1003. https://doi.org/10.1016/j.jhep.2011.02.015.
8. Mashizi MK, Tabaraei A. 2020. Study of the Effect of HBX gene of hepatitis B virus on liver cancer progress. Entomology and Applied Science Letters. 7:55–65.
9. Ali A, Abdel-Hafiz H, Suhail M, Al-Mars A, Zakaria MK, Fatima K, Ahmad S, Azhar E, Chaudhary A, Qadri I. 2014. Hepatitis B virus, HBx mutants and their role in hepatocellular carcinoma. World J Gastroenterol 20:10238–10248. https://doi.org/10.3748/wjg.v20.i30.10238.
10. Yu L, Zeng Z, Tan H, Feng Q, Zhou Q, Hu J, Li Y, Wang J, Yang W, Feng J, Xu B. 2022. Significant metabolic alterations in patients with hepatitis B virus replication observed via serum untargeted metabolomics shed new light on hepatitis B virus infection. J Drug Target 30:442–449. https://doi.org/10.1080/1061186X.2021.2009841.
11. Lamontagne RJ, Casciano JC, Bouchard MJ. 2018. A broad investigation of the HBV-mediated changes to primary hepatocyte physiology reveals HBV significantly alters metabolic pathways. Metabolism 83:50–59. https://doi.org/10.1016/j.metabol.2018.01.007.
12. Yang F, Yan S, He Y, Wang F, Song S, Guo Y, Zhou Q, Wang Y, Lin Z, Yang Y, Zhang W, Sun S. 2008. Expression of hepatitis B virus proteins in transgenic mice alters lipid metabolism and induces oxidative stress in the liver. J Hepatol 48:12–19. https://doi.org/10.1016/j.jhep.2007.06.021.
13. Schoeman JC, Hou J, Harms AC, Vreeken RJ, Berger R, Hankemeier T, Boonstra A. 2016. Metabolic characterization of the natural progression of chronic hepatitis B. Genome Med 8:64. https://doi.org/10.1186/s13073-016-0318-8.
14. Mráček T, Drahota Z, Houštěk J. 2013. The function and the role of the mitochondrial glycerol-3-phosphate dehydrogenase in mammalian tissues. Biochim Biophys Acta 1827:401–410. https://doi.org/10.1016/j.bbabio.2012.11.014.
15. Madiraju AK, Erion DM, Rahimi Y, Zhang X-M, Braddock DT, Albright RA, Prigaro BJ, Wood JL, Bhanot S, MacDonald MJ, Jurczak MJ, Camporez J-P, Lee H-Y, Cline GW, Samuel VT, Kibbey RG, Shulman GI. 2014. Metformin suppresses gluconeogenesis by inhibiting mitochondrial glycerophosphate dehydrogenase. Nature 510:542–546. https://doi.org/10.1038/nature13270.
16. Zheng Y, Qu H, Xiong X, Wang Y, Liu X, Zhang L, Liao X, Liao Q, Sun Z, Ouyang Q, Yang G, Zhu Z, Xu J, Zheng H. 2019. Deficiency of Mitochondrial Glycerol 3-Phosphate Dehydrogenase Contributes to Hepatic Steatosis. Hepatology 70:84–97. https://doi.org/10.1002/hep.30507.
17. Zhou M, Zhao K, Yao Y, Yuan Y, Pei R, Wang Y, Chen J, Hu X, Zhou Y, Chen X, Wu C. 2017. Productive HBV infection of well-differentiated, hNTCP-expressing human hepatoma-derived (Huh7) cells. Virol Sin 32:465–475. https://doi.org/10.1007/s12250-017-3983-x.
18. Gudayol M, Fabregat ME, Rasschaert J, Sener A, Malaisse WJ, Gomis R. 2002. Site-directed mutations in the FAD-binding domain of glycerophosphate dehydrogenase: catalytic defects with preserved mitochondrial anchoring of the enzyme in transfected COS-7 cells. Mol Genet Metab 75:168–173. https://doi.org/10.1006/mgme.2001.3286.
19. Gudayol M, Vidal J, Usac EF, Morales A, Fabregat ME, Fernández-Checa JC, Novials A, Gomis R. 2001. Identification and functional analysis of mutations in FAD-binding domain of mitochondrial glycerophosphate dehydrogenase in caucasian patients with type 2 diabetes mellitus. Endo 16:39–42. https://doi.org/10.1385/ENDO:16:1:39.
20. Lehn DA, Brown LJ, Simonson GD, Moran SM, MacDonald MJ. 1994. The sequence of a human mitochondrial glycerol-3-phosphate dehydrogenase-encoding cDNA. Gene 150:417–418. https://doi.org/10.1016/0378-1119(94)90469-3.
21. Szargel R, Shani V, Abd Elghani F, Mekies LN, Liani E, Rott R, Engelender S. 2016. The PINK1, synphilin-1 and SIAH-1 complex constitutes a novel mitophagy pathway. Hum Mol Genet 25:3476–3490. https://doi.org/10.1093/hmg/ddw189.
22. Yoo Y-S, Park Y-J, Lee H-S, Oanh NTK, Cho M-Y, Heo J, Lee E-S, Cho H, Park Y-Y, Cho H. 2019. Mitochondria ubiquitin ligase, MARCH5 resolves hepatitis B virus X protein aggregates in the liver pathogenesis. Cell Death Dis 10:938. https://doi.org/10.1038/s41419-019-2175-z.
23. Liu B, Zhang M, Chu H, Zhang H, Wu H, Song G, Wang P, Zhao K, Hou J, Wang X, Zhang L, Gao C. 2017. The ubiquitin E3 ligase TRIM31 promotes aggregation and activation of the signaling adaptor MAVS through Lys63-linked polyubiquitination. Nat Immunol 18:214–224. https://doi.org/10.1038/ni.3641.
24. Lv Z, Guo Y. 2020. Metformin and its benefits for various diseases. Front Endocrinol 11. https://doi.org/10.3389/fendo.2020.00191.
25. Xun Y-H, Zhang Y-J, Pan Q-C, Mao R-C, Qin Y-L, Liu H-Y, Zhang Y-M, Yu Y-S, Tang Z-H, Lu M-J, Zang G-Q, Zhang J-M. 2014. Metformin inhibits hepatitis B virus protein production and replication in human hepatoma cells. J Viral Hepat 21:597–603. https://doi.org/10.1111/jvh.12187.
26. Slagle BL, Bouchard MJ. 2016. Hepatitis B Virus X and Regulation of Viral Gene Expression. Cold Spring Harb Perspect Med 6:a021402. https://doi.org/10.1101/cshperspect.a021402.
27. Shin D, Kim SI, Kim M, Park M. 2006. Inhibition of hepatitis B virus replication by small interfering RNAs targeted to the viral X gene in mice. Virus Res 119:146–153. https://doi.org/10.1016/j.virusres.2005.12.012.
28. Kim G-W, Siddiqui A. Hepatitis B virus X protein recruits methyltransferases to affect cotranscriptional N6-methyladenosine modification of viral/host RNAs. 118:e2019455118. https://doi.org/10.1073/pnas.2019455118.
29. Han Q, Zhang C, Zhang J, Tian Z. 2011. Involvement of activation of PKR in HBx-siRNA-mediated innate immune effects on HBV inhibition. PLoS One 6:e27931. https://doi.org/10.1371/journal.pone.0027931.
30. Cheng S-T, Hu J-L, Ren J-H, Yu H-B, Zhong S, Wai Wong VK, Kwan Law BY, Chen W-X, Xu H-M, Zhang Z-Z, Cai X-F, Hu Y, Zhang W-L, Long Q-X, Ren F, Zhou H-Z, Huang A-L, Chen J. 2021. Dicoumarol, an NQO1 inhibitor, blocks cccDNA transcription by promoting degradation of HBx. J Hepatol 74:522–534. https://doi.org/10.1016/j.jhep.2020.09.019.
31. Tan G, Yi Z, Song H, Xu F, Li F, Aliyari R, Zhang H, Du P, Ding Y, Niu J, Wang X, Su L, Qin FX-F, Cheng G. 2019. Type-I-IFN-stimulated gene TRIM5γ inhibits HBV replication by promoting HBx degradation. Cell Rep 29:3551–3563.e3. https://doi.org/10.1016/j.celrep.2019.11.041.

32. Xu F, Song H, Xiao Q, Li N, Zhang H, Cheng G, Tan G. 2019. Type III interferon-induced CBFβ inhibits HBV replication by hijacking HBx. Molecular Immunology 16: 357–366. https://doi.org/10.1038/s41423-018-0006-2.
33. Xu F, Song H, Xiao Q, Wei Q, Pang X, Gao Y, Tan G. 2022. Type-III interferon stimulated gene TRIM31 mutation in an HBV patient blocks its ability in promoting HBx degradation. Virus Res 308:198650. https://doi.org/10.1016/j.virusres.2021.198650.
34. Tan G, Xu F, Song H, Yuan Y, Xiao Q, Ma F, Qin FX-F, Cheng G. 2018. Identification of TRIM14 as a type I IFN-stimulated gene controlling hepatitis B virus replication by targeting HBx. Front Immunol 9:1872. https://doi.org/10.3389/fimmu.2018.01872.
35. Kornyeyev D, Ramakrishnan D, Voitenleitner C, Livingston CM, Xing W, Hung M, Kwon HJ, Fletcher SP, Beran RK. 2019. Spatiotemporal analysis of hepatitis B Virus X protein in primary human hepatocytes. J Virol 93: e00248-19. https://doi.org/10.1128/JVI.00248-19.
36. Liu N, Zhang J, Yang X, Jiao T, Zhao X, Li W, Zhu J, Yang P, Jin J, Peng J, Li Z, Ye X. 2017. HDM2 promotes NEDDylation of hepatitis B virus HBx to enhance its stability and function. J Virol 91:e00340-17. https://doi.org/10.1128/JVI.00340-17.
37. Wan T, Lei Z, Tu B, Wang T, Wang J, Huang F. 2021. NEDD4 induces K48-linked degradative ubiquitination of hepatitis B virus X protein and inhibits HBV-associated HCC progression. Front Oncol 11:625169. https://doi.org/10.3389/fonc.2021.625169.
38. Song Y, Li M, Wang Y, Zhang H, Wei L, Xu W. 2021. E3 ubiquitin ligase TRIM21 restricts hepatitis B virus replication by targeting HBx for proteasomal degradation. Antiviral Res 192:105107. https://doi.org/10.1016/j.antiviral.2021.105107.
39. Zhao J, Wu J, Cai H, Wang D, Yu L, Zhang W-H. 2016. E3 ubiquitin ligase Siah-1 is down-regulated and fails to target natural HBx truncates for degradation in hepatocellular carcinoma. J Cancer 7:418–426. https://doi.org/10.7150/jca.13019.
40. Song H, Xu F, Xiao Q, Tan G. 2021. Hepatitis B virus X protein and its host partners. Cell Mol Immunol 18:1345–1346. https://doi.org/10.1038/s41423-021-00674-z.
41. Kamiński MM, Sauer SW, Kamiński M, Opp S, Ruppert T, Grigaravičius P, Grudnik P, Gröne H-J, Krammer PH, Gülow K. 2012. T cell activation is driven by an ADP-dependent glucokinase linking enhanced glycolysis with mitochondrial reactive oxygen species generation. Cell Rep 2: 1300–1315. https://doi.org/10.1016/j.celrep.2012.10.009.
42. Yu D-Y. 2020. Relevance of reactive oxygen species in liver disease observed in transgenic mice expressing the hepatitis B virus X protein. Lab Anim Res 36:6. https://doi.org/10.1186/s42826-020-00037-1.
43. Zhang Y, Li L, Cheng S-T, Qin Y-P, He X, Li F, Wu D-Q, Ren F, Yu H-B, Liu J, Chen J, Ren J-H, Zhang Z-Z. 2022. Rapamycin inhibits hepatitis B virus covalently closed circular DNA transcription by enhancing the ubiquitination of HBx. Front Microbiol 13:850087. https://doi.org/10.3389/fmicb.2022.850087.
44. Sekiba K, Otsuka M, Ohno M, Yamagami M, Kishikawa T, Suzuki T, Ishibashi R, Seimiya T, Tanaka E, Koike K. 2019. Inhibition of HBV Transcription From cccDNA With Nitazoxanide by Targeting the HBx–DDB1 Interaction. Cell Mol Gastroenterol Hepatol 7:297–312. https://doi.org/10.1016/j.jcmgh.2018.10.010.
45. Yuan Y, Zhao K, Yao Y, Liu C, Chen Y, Li J, Wang Y, Pei R, Chen J, Hu X, Zhou Y, Wu C, Chen X. 2019. HDAC11 restricts HBV replication through epigenetic repression of cccDNA transcription. Antiviral Res 172:104619. https://doi.org/10.1016/j.antiviral.2019.104619.
46. Chen Y, Yao Y, Zhao K, Liu C, Yuan Y, Sun H, Huang D, Zheng Y, Zhou Y, Chen J, Wang Y, Wu C, Zhang B, Guan Y, Li F, Pei R, Chen X. 2022. DNA repair factor poly(ADP-ribose) polymerase 1 is a proviral factor in hepatitis B virus covalently closed Circular DNA formation. J Virol 96:50. https://doi.org/10.1128/jvi.00585-22.
47. Sommer G, van Bömmel F, Will H. 2000. Genotype-specific synthesis and secretion of spliced hepatitis B virus genomes in hepatoma cells. Virology 271:371–381. https://doi.org/10.1006/viro.2000.0331.
48. Zhao K, Liu S, Chen Y, Yao Y, Zhou M, Yuan Y, Wang Y, Pei R, Chen J, Hu X, Zhou Y, Zhao H, Lu M, Wu C, Chen X. 2018. Upregulation of HBV transcription by sodium taurocholate cotransporting polypeptide at the postentry step is inhibited by the entry inhibitor Myrcludex B. Emerging Microbes & Infections 7:1–14. https://doi.org/10.1038/s41426-018-0189-8.
49. Lin Y, Wu C, Wang X, Liu S, Zhao K, Kemper T, Yu H, Li M, Zhang J, Chen M, Zhu Y, Chen X, Lu M. 2020. Glucosamine promotes hepatitis B virus replication through its dual effects in suppressing autophagic degradation and inhibiting MTORC1 signaling. Autophagy 16:548–561. https://doi.org/10.1080/15548627.2019.1632104.
50. Yao Y, Yang B, Chen Y, Wang H, Hu X, Zhou Y, Gao X, Lu M, Niu J, Wen Z, Wu C, Chen X. 2019. RNA-binding motif protein 24 (RBM24) is involved in pregenomic rna packaging by mediating interaction between hepatitis B virus polymerase and the epsilon element. J Virol 93:e02161-18. https://doi.org/10.1128/JVI.02161-18.
51. Zhao K, Wu C, Yao Y, Cao L, Zhang Z, Yuan Y, Wang Y, Pei R, Chen J, Hu X, Zhou Y, Lu M, Chen X. 2017. Ceruloplasmin inhibits the production of extracellular hepatitis B virions by targeting its middle surface protein. J Gen Virol 98:1410–1421. https://doi.org/10.1099/jgv.0.000794.
52. Yu K, He Y, Yeung LWY, Lam PKS, Wu RSS, Zhou B. 2008. DE-71-Induced apoptosis involving intracellular calcium and the Bax-mitochondria-caspase protease pathway in human neuroblastoma cells in vitro. Toxicol Sci 104:341–351. https://doi.org/10.1093/toxsci/kfn088.